Reactive Collision Avoidance for Nonholonomic Vehicles in Dynamic Environments with Obstacles of Arbitrary Shape ⋆

Aurora Haraldsen* Martin S. Wiig** Kristin Y. Pettersen*,**

*Centre for Autonomous Marine Operations and Systems (NTNU AMOS), Department of Engineering Cybernetics, Norwegian University of Science and Technology, Trondheim, Norway (e-mail: aurora.haraldsen@ntnu.no).
**Norwegian Defence Research Establishment (FFI), Kjeller, Norway. (e-mail: martin-syre.wiig@ffi.no)

Abstract: Over the recent years, there has been an increasing interest in autonomous systems. Consequently, the problem of avoiding static and dynamic obstacles without human interference has gained a lot of attention. Avoiding collision, even in completely static environments, is significantly more challenging when the vehicle is subject to nonholonomic constraints. This paper presents a reactive algorithm for collision avoidance of dynamic, arbitrarily shaped obstacles, which is suitable for unicycle-type, nonholonomic vehicles. Unlike most reactive methods, we consider the exact shape of the obstacle, which allows the vehicle to utilize any space that is not occupied by the obstacle. This is an advantage over circle and ellipse approximations, as they can lead to overly conservative maneuvers. We provide explicit conditions under which collision avoidance is mathematically proven and validate the analysis by numerical simulations.

Keywords: Autonomous vehicles; collision avoidance; nonholonomic constraints; real-time control; nonlinear dynamical systems

1. INTRODUCTION

Autonomous vehicles are required to venture into unknown environments, where they may encounter both static and dynamic obstacles. Collision avoidance algorithms are generally divided into two categories: global and local. Global techniques, often used interchangeably with *motion planning*, describe algorithms that compute a complete path to the goal prior to execution and therefore typically require an extensive world model. In unknown, dynamic environments, the applicability of planning algorithms is, however, greatly reduced. Even if some knowledge of the conditions is possible to obtain, the model is likely erroneous or incomplete. In any case, it is crucial that the vehicle is able to deal with unexpected changes in its surroundings, as the consequences of a collision may be fatal. Hence, there is need for a local navigation scheme. Local or *reactive* methods are based on computing the next control command using the current, local measurements at each sampling instance. The vehicle can therefore react quickly to new information, which is advantageous when venturing into unpredictable conditions. Reactive algorithms are easily combined with other goal-reaching behaviour, like following a global path, but also work well as the sole navigation method during smaller missions.

Today's obstacle detection systems are highly developed. For measuring the obstacle shape, computer vision algorithms using one or several cameras are becoming increasingly common. Technology such as radars, lidars, and ultrasonic sensors can be used for this purpose as well. Having knowledge of the obstacle shape it is possible to use this as an advantage when avoiding collision. However, most methods which consider dynamic obstacles are either based on approximating the obstacle as a circular domain, e.g. Savkin and Wang (2013); López et al. (2020); Poonganam et al. (2020), as a point from which the vehicle must maintain a constant distance such as Moe et al. (2020); Li and Zheng (2020); Zhang et al. (2013), or require extensive calculations as in Seder and Petrovic (2007) and can therefore not be applied reactively. The circle approximation is computationally simple, but can yield overly conservative maneuvers. This particularly occurs when the obstacle size is considerably greater along one dimension compared to the other. A more accurate approximation is then the ellipse (Choi et al., 2006; Zhu et al., 2020), which provides two parameters that can be adjusted to fit the obstacle shape. However, this approximation removes some of the computational advantages of the circle and will still yield conservative maneuvers if the shape is non-convex.

Some methods do not fall into the above mentioned categories. The collision cone approach (Chakravarthy and Ghose, 1998) can handle two objects of arbitrary shape, which is extended to deforming shapes in Sunkara et al.

(2019), but assumes the objects to move/deform with constant velocities. The approach is developed further in Sunkara and Chakravarthy (2016) to also consider time-varying velocities of non-deforming objects. A drawback is, however, that the resulting guidance law contains several singularities. Furthermore, the method does not account for nonholonomic constraints, which may make it impossible for the vehicle to implement the given commands. The method given in Savkin and Wang (2014) represents a reactive navigation approach based on an integrated environment representation, which provably ensures vehicle safety in a complex environment with several moving obstacles. However, the method does not consider the obstacle velocities and can therefore lead to maneuvers that are more conservative than necessary when velocity measurements are available. The approaches given in Zhu et al. (2012); Masehian and Katebi (2007); Xinyi et al. (2019) do not provide a mathematical analysis of the algorithm, nor do the methods in Zhu et al. (2012); Masehian and Katebi (2007) account for nonholonomic constraints.

In this paper, we propose a reactive method for avoiding dynamic obstacles of arbitrary shape, which is suitable for unicycle-type, nonholonomic vehicles. The proposed solution adapts the collision cone concept to make the vehicle avoid potential collisions. We have previously presented a reactive collision avoidance strategy of circularly shaped obstacles based on this concept (Haraldsen et al., 2020), which provably ensures safety of a nonholonomic vehicle with speed and turning constraints. However, the obstacle shape cannot always be properly described by a circle. Indeed, this approximation can cause the obstacle to occupy considerably more space than necessary. Therefore, in this work, we improve the algorithm to handle arbitrarily shaped obstacles which may still be dynamic and even strictly non-cooperative. In the circular case, the collision avoidance problem is significantly less complex. The vehicle must in that case keep a safe distance to the obstacle center, and the obstacle is thus effectively modeled as a point mass. To compensate for the obstacle's movement, the velocity of the center can be considered exclusively. For non-circular obstacles, the control problem instead involves keeping the vehicle a safe distance from the obstacle boundary. This is a more difficult scenario for several reasons, e.g. since the velocity of the obstacle along its boundary differ depending on the distance to its center of rotation and may be significantly greater than that of the center. By considering these matters, however, we are able to find a solution which achieves the desired vehicle behaviour. The resulting algorithm generates less conservative maneuvers, which is a major advantage, especially in crowded environments. Specifically, it allows the vehicle to stay closer to the boundary of non-circular objects while still preserving the required minimum safety distance. Through a rigorous mathematical analysis, the algorithm is shown to guarantee collision avoidance for a nonholonomic vehicle which moves at a constant speed and has an explicitly bounded turning rate.

The paper is organized as follows. Section 2 presents the system models. In Section 3 we define the conditions under which collision avoidance of a dynamic, arbitrarily shaped obstacle is ensured. These conditions are the basis for the collision avoidance algorithm presented in Section 4.

Numerical simulations are provided in Section 5, before some concluding remarks are given in Section 6.

2. MATHEMATICAL MODELING

This section presents the mathematical models of a non-holonomic vehicle and an arbitrarily shaped, dynamic obstacle.

2.1 Vehicle model

We consider the nonholonomic vehicle,

$$\dot{x}_v = u_v \cos(\psi_v), \tag{1a}$$
$$\dot{y}_v = u_v \sin(\psi_v), \tag{1b}$$
$$\dot{\psi}_v = r_v, \tag{1c}$$

where $\boldsymbol{p}_v \triangleq \langle x_v, y_v \rangle$ are the Cartesian coordinates of the vehicle, $\boldsymbol{v}_v \triangleq \dot{\boldsymbol{p}}_v$ is the linear velocity, and ψ_v is the heading angle. Moreover, u_v is the forward speed and r_v is the heading rate.

Assumption 1. The forward speed, $u_v > 0$, is constant. The turning rate, r_v, is directly controlled and bounded by

$$r_v \in [-r_{v,\max}, r_{v,\max}], \tag{2}$$

where $r_{v,\max} > 0$ is a constant parameter.

2.2 Obstacle model

We consider a dynamic obstacle of arbitrary shape, represented by a moving domain $\mathcal{D}_o$. Let o denote the obstacle attached reference frame, which has the position $\boldsymbol{p}_o \triangleq \langle x_o, y_o \rangle$ and the orientation ψ_o. The obstacle is modeled by the following set of equations:

$$\dot{x}_o = u_o \cos(\psi_o), \tag{3a}$$
$$\dot{y}_o = u_o \sin(\psi_o), \tag{3b}$$
$$\dot{\psi}_o = r_o, \tag{3c}$$
$$\dot{u}_o = a_o, \tag{3d}$$
$$\dot{r}_o = \alpha_o, \tag{3e}$$

where u_o and a_o are the forward speed and acceleration of the obstacle, respectively, and r_o and α_o are the angular velocity and acceleration of the obstacle about $\boldsymbol{p}_o$.

Assumption 2. The domain $\mathcal{D}_o$ is rigid and has a piecewise smooth boundary $\partial \mathcal{D}_o$.

Assumption 2 implies that the obstacle domain cannot be deformed and that its boundary is continuous. We now state some necessary assumptions regarding the model (3).

Assumption 3. The forward speed, u_o, and the forward acceleration, a_o, are bounded by

$$u_o \in [0, u_{o,\max}], \tag{4}$$
$$a_o \in [-a_{o,\max}, a_{o,\max}], \tag{5}$$

where $u_{o,\max} \geq 0$ and $a_{o,\max} \geq 0$ are constant parameters.

Assumption 4. The angular velocity, r_o, and the angular acceleration, α_o, are bounded by

$$r_o \in [-r_{o,\max}, r_{o,\max}], \tag{6}$$
$$\alpha_o \in [-\alpha_{o,\max}, \alpha_{o,\max}], \tag{7}$$

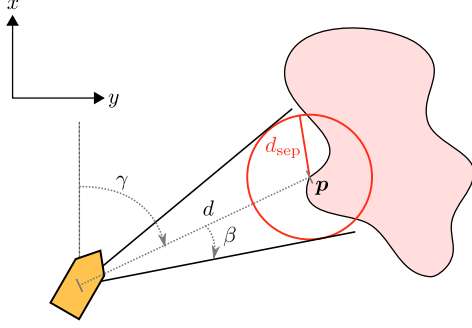where $r_{o,\max} \geq 0$ and $\alpha_{o,\max} \geq 0$ are constant parameters.

Fig. 1. The angles γ and β, and the distance d.

3. OBSTACLE AVOIDANCE

This section establishes the conditions under which the vehicle keeps a safe distance to the obstacle boundary, avoiding a collision by the following definition:

Definition 1. (Collision). A collision occurs between the vehicle and the obstacle if $d_{vo} < d_{\text{sep}}$, where $d_{\text{sep}} > 0$ is a minimum separation distance and $d_{vo} \triangleq \min_{\boldsymbol{p} \in \partial \mathcal{D}_o} \|\boldsymbol{p}_v - \boldsymbol{p}\|$.

Lemma 1. Consider an obstacle modeled by (3). Suppose that the vehicle (1) maintains a velocity satisfying

$$|\psi_{v\boldsymbol{p}} - \gamma_v(\boldsymbol{p})| \geq \beta_v(\boldsymbol{p}) \,\forall\, \boldsymbol{p} \in \partial \mathcal{D}_o, \tag{8}$$

where $\psi_{v\boldsymbol{p}} \triangleq \text{atan2}\,(\boldsymbol{v}_v - \dot{\boldsymbol{p}})$, $\gamma_v(\boldsymbol{p}) \triangleq \text{atan2}\,(\boldsymbol{p} - \boldsymbol{p}_v)$, and

$$\beta_v(\boldsymbol{p}) \triangleq \sin^{-1}\left(\frac{d_{\text{sep}}}{\|\boldsymbol{p}_v - \boldsymbol{p}\|}\right), \tag{9}$$

for all $t \geq t_0$, and suppose that the vehicle starts in a collision-free state. Then, the vehicle will avoid a collision with the obstacle, that is

$$d_{vo}(t) \geq d_{\text{sep}} \,\forall\, t \geq t_0. \tag{10}$$

Remark 1. The operation $\text{atan2}(\boldsymbol{n})$, where $\boldsymbol{n} \triangleq \langle n_x, n_y \rangle \in \mathbb{R}^2$, is computed as $\text{atan2}(n_y, n_x)$ following the standard notation of the atan2 function.

Proof. The geometry of the proof is illustrated in Figure 1. The vehicle maintains a relative velocity $\boldsymbol{v}_{v\boldsymbol{p}} \triangleq \boldsymbol{v}_v - \dot{\boldsymbol{p}}$ and heading $\psi_{v\boldsymbol{p}} \triangleq \text{atan2}\,(\boldsymbol{v}_v - \dot{\boldsymbol{p}})$ with respect to a point $\boldsymbol{p} \in \partial \mathcal{D}_o$ on the obstacle boundary. The line-segment going from the vehicle position, $\boldsymbol{p}_v$, to $\boldsymbol{p}$ has the length $d \triangleq \|\boldsymbol{p}_v - \boldsymbol{p}\|$ and the orientation $\gamma \triangleq \gamma_v(\boldsymbol{p})$. The time-derivative of the distance, d, is found geometrically as

$$\dot{d} = -\|\boldsymbol{v}_{v\boldsymbol{p}}\| \cos(\psi_{v\boldsymbol{p}} - \gamma). \tag{11}$$

By (8) and (11), we obtain

$$\dot{d} \geq -\|\boldsymbol{v}_{v\boldsymbol{p}}\| \sqrt{1 - \left(\frac{d_{\text{sep}}}{d}\right)^2}, \tag{12}$$

where we have inserted the expression for $\beta \triangleq \beta_v(\boldsymbol{p})$ given by (9). Computing the differential equation (12) yields

$$\sqrt{d(t)^2 - d_{\text{sep}}^2} - \sqrt{d(t_0)^2 - d_{\text{sep}}^2} \geq -\int_{t_0}^{t} \|\boldsymbol{v}_{v\boldsymbol{p}}(\tau)\| d\tau, \tag{13}$$

which can be solved for d,

$$d(t) \geq \sqrt{\left(\sqrt{d(t_0)^2 - d_{\text{sep}}^2} - \int_{t_0}^{t} \|\boldsymbol{v}_{v\boldsymbol{p}}(\tau)\| d\tau\right)^2 + d_{\text{sep}}^2}. \tag{14}$$

Since (14) holds for any point on the obstacle boundary, the vehicle will keep at least a distance d_{sep} to the obstacle.
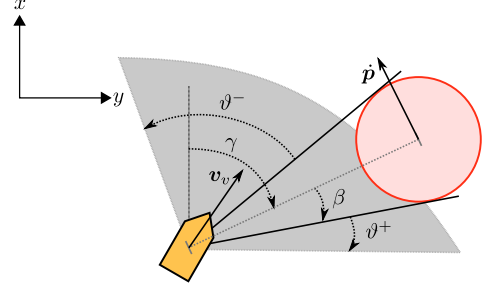

Fig. 2. The angles $\vartheta^{\pm}$ and the set $\mathcal{E}(\boldsymbol{p})$.

Remark 2. The condition (8) corresponds to the vehicle maintaining a relative velocity outside of the collision cone, as demonstrated for a single point in Figure 1, for all points on the boundary of the obstacle domain.

3.1 Turning requirement

To compensate for the velocity $\dot{\boldsymbol{p}}$, we rotate the edges of the collision cone, depicted in Figure 1, by the angles

$$\vartheta^{\pm}(\boldsymbol{p}) \triangleq \sin^{-1}\left(\frac{\|\dot{\boldsymbol{p}}\|}{u_v} \sin\left(\eta^{\pm}(\boldsymbol{p})\right)\right), \tag{15}$$

as illustrated in Figure 2, where

$$\eta^{\pm}(\boldsymbol{p}) \triangleq \gamma_v(\boldsymbol{p}) \pm \beta_v(\boldsymbol{p}) + \pi - \psi_{\boldsymbol{p}}, \tag{16}$$

and we denote the orientation of the vector $\dot{\boldsymbol{p}}$ as $\psi_{\boldsymbol{p}} \triangleq \text{atan2}(\dot{\boldsymbol{p}})$. The set $\mathcal{E}(\boldsymbol{p}) \triangleq \left(\xi^-(\boldsymbol{p}), \xi^+(\boldsymbol{p})\right)$ is shown as the grey, shaded area in Figure 2, where

$$\xi^{\pm}(\boldsymbol{p}) \triangleq \gamma_v(\boldsymbol{p}) \pm \beta_v(\boldsymbol{p}) + \vartheta^{\pm}(\boldsymbol{p}). \tag{17}$$

The transformation is derived in Haraldsen et al. (2020). An equivalent condition to (8) is thus

$$\psi_v \notin \mathcal{E}(\boldsymbol{p}) \,\forall\, \boldsymbol{p} \in \partial \mathcal{D}_o. \tag{18}$$

For the purpose of the next lemma, define the distances from the vehicle heading to this set, given by

$$\Delta^{\pm}(\boldsymbol{p}) \triangleq \pm \psi_v \mp \xi^{\pm}(\boldsymbol{p}). \tag{19}$$

The angles, adapted from Lalish et al. (2008), are wrapped into the domain $\Delta^{\pm}(\boldsymbol{p}) \in (-2\pi, 2\pi]$ such that the distances are positive when $\psi_v \notin \mathcal{E}(\boldsymbol{p})$ and negative otherwise. Moreover, the shortest distance is found geometrically as

$$\Delta^{\min}(\boldsymbol{p}) \triangleq \begin{cases} \Delta^+(\boldsymbol{p}) & \text{if } \psi_{v\boldsymbol{p}} - \gamma_v(\boldsymbol{p}) \geq 0, \\ \Delta^-(\boldsymbol{p}) & \text{if } \psi_{v\boldsymbol{p}} - \gamma_v(\boldsymbol{p}) < 0, \end{cases} \tag{20}$$

where we map the angular difference to the interval $(\psi_{v\boldsymbol{p}} - \gamma_v(\boldsymbol{p})) \in (-\pi, \pi]$. Before stating the next lemma, which derives a maximum turning requirement, define the constants $u_{\max} \triangleq u_{o,\max} + r_{o,\max} d_{\max}$ and $a_{\max} \triangleq a_{o,\max} + \alpha_{o,\max} d_{\max}$, where $d_{\max} \triangleq \max_{\boldsymbol{p} \in \partial \mathcal{D}_o} \|\boldsymbol{p}_o - \boldsymbol{p}\|$.

Lemma 2. Let Assumption 1 through 4 hold. Suppose that the vehicle (1) at some time $t_1 \geq t_0$ satisfies condition (8) of Lemma 1 and $d_{vo}(t_1) \geq d_{\text{sep}}$. Furthermore, suppose that the vehicle maintains a turning rate satisfying

$$\begin{aligned} \Delta_o^+ = 0 &\implies r_v = r_{v,\max} \\ \Delta_o^- = 0 &\implies r_v = -r_{v,\max} \end{aligned} \tag{21}$$

for all $t \geq t_1$, where

$$\Delta_o^{\pm} \triangleq \min_{\boldsymbol{p} \in \partial \mathcal{D}_o} \Delta^{\pm}(\boldsymbol{p}) \tag{22}$$

and the maximum turning rate is lower bounded by

$$r_{v,\max} \geq r_{o,\max} \frac{u_{\max}}{u_v} + \frac{a_{\max}}{\sqrt{u_v^2 - u_{\max}^2}}. \tag{23}$$

Then, under the following assumption:

Assumption 5. The forward speed, u_v, is bounded by

$$u_v > u_{\max}. \tag{24}$$

the vehicle will remain out of collision with the obstacle (3), that is $d_{vo}(t) \geq d_{\text{sep}} \, \forall \, t \geq t_1$.

Proof.

Define $\Delta^\pm \triangleq \Delta^\pm(\boldsymbol{p})$, $\gamma \triangleq \gamma_v(\boldsymbol{p})$, $\beta \triangleq \beta_v(\boldsymbol{p})$, and $\vartheta^\pm \triangleq \vartheta^\pm(\boldsymbol{p})$ for conciseness. The time-derivative of $\Delta^\pm$ is

$$\dot{\Delta}^\pm = \pm r_v \mp \dot{\gamma} - \dot{\beta} \mp \dot{\vartheta}, \tag{25}$$

by (17). The time-derivative of γ is found geometrically as

$$\dot{\gamma} = -\frac{\|\boldsymbol{v}_{v\boldsymbol{p}}\|}{d} \sin(\psi_{v\boldsymbol{p}} - \gamma), \tag{26}$$

where $d \triangleq \|\boldsymbol{p}_v - \boldsymbol{p}\|$, and the time-derivative of β is

$$\dot{\beta} = \frac{\|\boldsymbol{v}_{v\boldsymbol{p}}\|}{d} \cos(\psi_{v\boldsymbol{p}} - \gamma) \tan(\beta), \tag{27}$$

computed from (9), where we have inserted the expression for $\dot{d}$. The time-derivative of $\vartheta^\pm$ is computed from (15) as

$$\dot{\vartheta}^\pm = (-r_o + \dot{\gamma} \pm \dot{\beta})F(\eta^\pm) + \frac{d\|\dot{\boldsymbol{p}}\|}{dt}G(\eta^\pm), \tag{28}$$

using that $\dot{\psi}_{\boldsymbol{p}} \triangleq r_o$, where $\eta^\pm \triangleq \eta^\pm(\boldsymbol{p})$ is defined in (16), and the following terms are defined for conciseness:

$$F(x) \triangleq \frac{\|\dot{\boldsymbol{p}}\|\cos(x)}{u_v\sqrt{1 - \left(\frac{\|\dot{\boldsymbol{p}}\|}{u_v}\right)^2 \sin^2(x)}}, \tag{29a}$$

$$G(x) \triangleq \frac{\sin(x)}{u_v\sqrt{1 - \left(\frac{\|\dot{\boldsymbol{p}}\|}{u_v}\right)^2 \sin^2(x)}}. \tag{29b}$$

By the above calculations, (25) may be written as

$$\dot{\Delta}^\pm = \pm r_v \pm r_o F\left(\eta^\pm\right) \mp \frac{d\|\dot{\boldsymbol{p}}\|}{dt}G\left(\eta^\pm\right) + \left(1 + F\left(\eta^\pm\right)\right)$$
$$\frac{\|v_{v\boldsymbol{p}}\|}{d}\left(\pm \sin\left(\psi_{v\boldsymbol{p}} - \gamma\right) - \cos\left(\psi_{v\boldsymbol{p}} - \gamma\right)\tan\left(\beta\right)\right). \tag{30}$$

The velocity of any point $\boldsymbol{p} \in \partial \mathcal{D}_o$ is computed as

$$\dot{\boldsymbol{p}} = \boldsymbol{v}_o + d_o r_o \left[-\sin(\phi) \ \cos(\phi)\right]^\top, \tag{31}$$

where $\boldsymbol{v}_o \triangleq \dot{\boldsymbol{p}}_o$, $d_o \triangleq \|\boldsymbol{p}_o - \boldsymbol{p}\|$, and $\phi \triangleq \text{atan2}(\boldsymbol{p} - \boldsymbol{p}_o)$. It is straight-forward to verify that $\|\dot{\boldsymbol{p}}\| \leq u_{\max}$ from (31). Thus, Assumption 5 ensures that the terms (29) are bounded and that (15) is well-defined. Recalling that the shortest distance, $\Delta^{\min} \triangleq \Delta^{\min}(\boldsymbol{p})$, satisfies (20), we have $\pm \sin(\psi_{v\boldsymbol{p}} - \gamma) = |\sin(\psi_{v\boldsymbol{p}} - \gamma)|$. This in combination with (8) entails $\pm \sin(\psi_{v\boldsymbol{p}} - \gamma) - \cos(\psi_{v\boldsymbol{p}} - \gamma)\tan(\beta) \geq 0$. Thus, seeing that $F\left(\eta^\pm\right) \in (-1, 1)$, we may reduce (30) to

$$\dot{\Delta}^\pm \geq \pm r_v \pm r_o F\left(\eta^\pm\right) \mp \frac{d\|\dot{\boldsymbol{p}}\|}{dt}G\left(\eta^\pm\right). \tag{32}$$

The term $\frac{d\|\dot{\boldsymbol{p}}\|}{dt}$ can similarly be bounded:

$$\frac{d\|\dot{\boldsymbol{p}}\|}{dt} = a_o \frac{(u_o + d_o r_o \sin(\psi_o - \phi))}{\sqrt{u_o^2 + (d_o r_o)^2 + 2d_o r_o u_o \sin(\psi_o - \phi)}} +$$
$$d_o \alpha_o \frac{(u_o \sin(\psi_o - \phi) + d_o r_o)}{\sqrt{u_o^2 + (d_o r_o)^2 + 2d_o r_o u_o \sin(\psi_o - \phi)}}, \tag{33}$$

where we employ that $\dot{\phi} = r_o$. It can easily be verified that $a_{\max}$ is an upper bound of (33). The rest of the terms in (32) are bounded by assumption. It follows that a turning rate, r_v, satisfying (21), where $r_{v,\max}$ is lower bounded by (23), ensures that $\dot{\Delta}_o^\pm \geq 0$, implying that $\Delta^\pm(\boldsymbol{p}) \geq \Delta_o^\pm \geq 0$ for all $\boldsymbol{p} \in \partial \mathcal{D}_o$ by (22), which ensures that condition (8) of Lemma 1 holds for all $t \geq t_1$.

4. COLLISION AVOIDANCE ALGORITHM

This section presents the collision avoidance (CA) algorithm. Based on the previous theory, we can strategically design the algorithm to ensure that collisions are avoided. Motivated by Wiig et al. (2017), the control system of the vehicle has two modes: nominal mode and collision avoidance mode. The control system switches between the two modes based on a set of safety conditions. An analysis of the proposed algorithm is given.

4.1 Nominal behaviour

Since obstacle avoidance is the main focus of this paper, we leave the nominal behaviour of the vehicle unspecified but assume for convenience that its nominal goal is to reach some target position $\boldsymbol{p}_t \triangleq \langle x_t, y_t \rangle$, which requires it to maintain a heading ψ_{nom}. Due to the modular structure of the algorithm, the nominal behaviour of the vehicle can easily be replaced with any other desired behaviour.

4.2 Switching conditions

The control system is switched from nominal mode to collision avoidance mode if the distance to the obstacle is reduced to a safety distance,

$$d_{vo} \leq d_{\text{safe}}, \tag{34}$$

simultaneously as the desired heading in nominal mode is unsafe, that is

$$\exists \, \boldsymbol{p} \in \partial \mathcal{D}_o \ni \psi_{\text{nom}} \in \mathcal{E}(\boldsymbol{p}). \tag{35}$$

The safety distance, $d_{\text{safe}} > 0$, is a design parameter but should be chosen large enough to guarantee that a collision is avoided. We will provide a lower bound of d_{safe} in Theorem 1. To avoid oscillations, the vehicle exits CA mode, and thus resumes its nominal behaviour, only if the nominal heading is safe to follow once more, that is

$$\psi_{\text{nom}} \notin \mathcal{E}(\boldsymbol{p}) \, \forall \, \boldsymbol{p} \in \partial \mathcal{D}_o. \tag{36}$$

4.3 Turning law

In CA mode, it is crucial that the vehicle maintains a safe heading, as the distance to the obstacle has been reduced to an undesired distance. The turning direction of the vehicle is determined as the vehicle enters CA mode and is held constant throughout the maneuver, chosen as

$$\text{dir} \triangleq \arg\min_{j \in \{\pm\}} \begin{cases} \Delta_o^j & \text{if } \Delta_o^\pm \geq 0, \\ \max_{\boldsymbol{p} \in \partial \mathcal{D}_o} \left|\Delta^j(\boldsymbol{p})\right| & \text{otherwise}, \end{cases} \tag{37}$$

where the distances $\Delta_o^\pm$ are defined in (22). The parameter (37) is chosen to satisfy the turning criteria (21) of Lemma 2 when the vehicle maintains a safe heading by condition (8). If this is not the case, then the turning

direction is chosen to make the vehicle take the shortest turn to a safe heading. The turning rate is moreover chosen as

$$r_v = \begin{cases} \pm r_{v,\max} & \text{if } \Delta_o^{\pm} \le \Delta_{\text{safe}} \mid \text{dir} = \pm, \\ 0 & \text{otherwise,} \end{cases} \quad (38)$$

where $\Delta_{\text{safe}} \ge 0$ is a constant design parameter, which can be interpreted as an angular safety distance.

Remark 3. The intuition behind (38) comes from the formulation of $\Delta_o^{\pm}$ in (22) and the result of Lemma 2. If the vehicle maintains a safe heading, i.e. satisfies (8), then $\Delta_o^{\pm} \ge 0$ since $\Delta^{\pm}(\boldsymbol{p}) \ge 0$ for all $\boldsymbol{p} \in \partial \mathcal{D}_o$. In that case, the control input satisfies condition (21) of Lemma 2. If this is not the case, then we are guaranteed that there exists at least one point $\boldsymbol{p} \in \partial \mathcal{D}_o$ such that $\psi_v \in \mathcal{E}(\boldsymbol{p})$, rendering the associated distances negative, $\Delta^{\pm}(\boldsymbol{p}) < 0$, and thus the minimum (22) is negative, that is $\Delta_o^{\pm} < 0$. This ensures by (38) that the vehicle will keep turning in the chosen direction as long as the vehicle maintains an unsafe heading. Note that, to generate a smooth trajectory and avoid chattering at $\Delta_o^{\pm} = \Delta_{\text{safe}}$, the control input (38) is implemented as a high-gain, proportional controller.

4.4 Analysis

Theorem 1. Under Assumption 1 through 5, the vehicle (1) following the collision avoidance algorithm, with the switching rules (34)-(36) and the turning law (38), will avoid a collision with the obstacle (3), that is

$$d_{vo}(t) \ge d_{\text{sep}} \,\forall\, t \ge t_0, \quad (39)$$

provided the initial distance to the obstacle satisfies $d_{vo}(t_0) \ge d_{\text{safe}}$, where

$$d_{\text{safe}} \ge \frac{2u_v + \pi u_{\max}}{r_{v,\max}} + d_{\text{sep}}, \quad (40)$$

and the following assumption holds:

Assumption 6. The maximum turning rate, $r_{v,\max}$, satisfies condition (23) of Lemma 2.

Proof.

If the vehicle is not in collision avoidance (CA) mode, it follows from the switching rules (34)-(36) that $d_{vo} > d_{\text{safe}}$ or condition (8) holds. It is obvious that (39) holds in the first case, and it is implied by Lemma 1 in the second case.

Suppose now that the vehicle enters CA mode at a time $t_1 \ge t_0$ as $d_{vo}(t_1) = d_{\text{safe}}$. If condition (8) does not hold at this time, then the vehicle will immediately start turning at the maximum rate to obtain a safe heading by (38). In order to obtain a safe heading, the required turn can at most be π rad since the vehicle takes the shortest turn by (37). Furthermore, the distance to any point $\boldsymbol{p} \in \partial \mathcal{D}_o$, moving with the velocity $\dot{\boldsymbol{p}}$, can at most be reduced by

$$\frac{2u_v + \pi u_{\max}}{r_{v,\max}} \quad (41)$$

during the time it takes for the vehicle to make a π rad turn, as shown in Wiig et al. (2017). Thus, by (40), there exists a time $t_2 > t_1$ at which the vehicle satisfies (8) and such that $d_{vo}(t) \ge d_{\text{sep}} \,\forall\, t \in [t_1, t_2]$. It follows from Lemma 2 and Assumption 6 that (39) holds thereafter.

Last, suppose that the vehicle enters CA mode at a time $t_3 > t_0$ while $d_{vo}(t_3) < d_{\text{safe}}$. At this time, the vehicle must
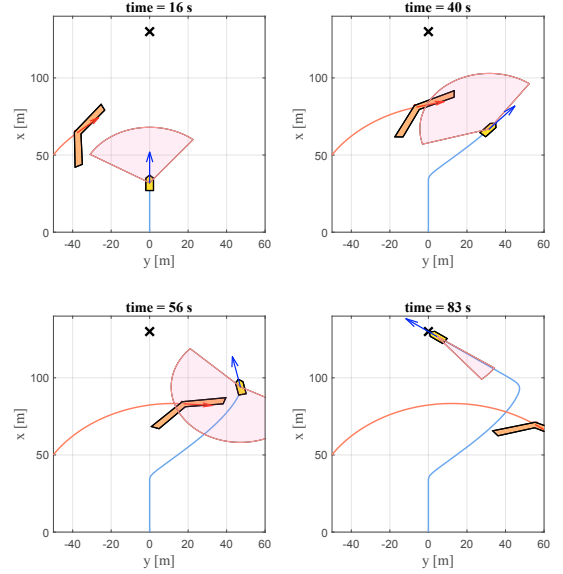
(a) North-East plots from the simulation. The vehicle and obstacle trajectories are given by the blue and red solid lines, respectively. The vehicle is the yellow polygon, and the obstacle is the orange polygon. The red, transparent sector represents the union of the sets $\mathcal{E}(\boldsymbol{p})$ along the obstacle boundary, with a radius of d_{safe}. The blue vector shows ψ_v, and the target position $\boldsymbol{p}_t$ is marked by an 'X'.
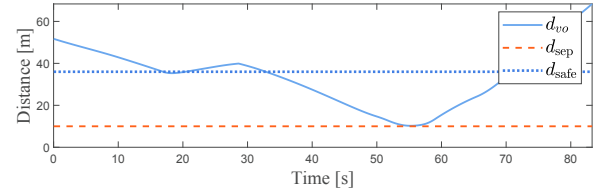
(b) Distance to the obstacle during the simulation.

Fig. 3. Simulation with a non-convex obstacle.

satisfy (8), otherwise the vehicle would have entered CA mode as $d_{vo} = d_{\text{safe}}$ by the switching criteria. It follows from the turning law (38), Lemma 2, and Assumption 6 that (39) holds. Thus, by the above reasoning, we can conclude that the vehicle will remain out of collision.

5. SIMULATION EXAMPLE

To demonstrate the algorithm and verify the mathematical analysis, we present a simulation of the vehicle (1) moving towards a static target, chosen as $\boldsymbol{p}_t = \langle 130, 0 \rangle$ m, in the presence of an obstacle modeled as a moving, rigid domain with the dynamics given by (3). The vehicle has a forward speed of $u_v = 2$ m/s and a maximum turning rate of $r_{v,\max} = 0.4$ rad/s. We choose $\Delta_{\text{safe}} = 0.1$ rad and $d_{\text{sep}} = 10$ m. The obstacle is represented by the simple polygon $P = \{\langle 21.5, 6 \rangle, \langle 18.5, 9 \rangle, \langle 0, 1.5\sqrt{2} \rangle, \langle -18.5, 9 \rangle, \langle -21.5, 6 \rangle, \langle 0, -1.5 \rangle\}$, given in meters with respect to the origin $\boldsymbol{p}_o$. The obstacle bounds are $a_{o,\max} = 0.1$ m/s^2, $u_{o,\max} = 1.5$ m/s, $r_{o,\max} = 0.02$ rad/s, and $\alpha_{o,\max} = 0$ rad/s^2. We choose $d_{\text{safe}} = 36$ m to satisfy (40).

The trajectories of the vehicle and the obstacle are shown in Figure 3a. At $t = 16$ s, the vehicle is closing in at the target as the obstacle approaches from the left. The vehicle enters CA mode in accordance with the switching rules (34)-(35) as $d_{vo} = d_{\text{safe}}$ and immediately turns right

by (37), in order to avoid a collision. The vehicle proceeds in this direction for some time by the turning law (38) while the obstacle moves towards it at high speed. The vehicle is eventually able to circumvent the obstacle and proceed to the target, as seen in the bottom two plots of Figure 3a. We can verify by Figure 3b that the distance, d_{vo}, remains above d_{sep} at all times, supporting the result of Theorem 1.

6. CONCLUSION

In this paper, we have presented a reactive algorithm for collision avoidance of a dynamic obstacle of arbitrary shape. The proposed method provably ensures avoidance of an obstacle that is able to change both its speed and direction at any instant, under explicit conditions derived by an analysis of the closed-loop system. The algorithm has the potential to generate less conservative vehicle maneuvers compared to methods that approximate the obstacle shape by a circle or an ellipse, especially when avoiding obstacles that are not well represented by such shapes, e.g. non-convex domains. As many physical systems are subject to kinematic constraints, which may limit their abilities to avoid collision, we apply the algorithm to a nonholonomic vehicle that is restricted to maintain a constant forward speed and has a bounded turning rate. Even under these constraints, we show that collision avoidance of a dynamic, arbitrarily shaped obstacle is guaranteed, provided the speed and maximum turning rate of the vehicle are sufficiently large. To verify the theoretical analysis, we provided a simulation of the vehicle moving towards a static target in the presence of a dynamic obstacle shaped as a non-convex polygon, confirming safety of the vehicle.

REFERENCES

Chakravarthy, A. and Ghose, D. (1998). Obstacle avoidance in a dynamic environment: a collision cone approach. *IEEE Transactions on Systems, Man, and Cybernetics*, 28(5), 562–574. doi:10.1109/3468.709600.

Choi, Y., Wang, W., Liu, Y., and Kim, M. (2006). Continuous collision detection for two moving elliptic disks. *IEEE Transactions on Robotics*, 22(2), 213–224. doi:10.1109/TRO.2005.862479.

Haraldsen, A., Wiig, M.S., and Pettersen, K.Y. (2020). Vehicle safety of the velocity obstacle algorithm. In *59th IEEE Conference on Decision and Control*, 5340–5347. doi:10.1109/CDC42340.2020.9304208.

Lalish, E., Morgansen, K.A., and Tsukamaki, T. (2008). Decentralized reactive collision avoidance for multiple unicycle-type vehicles. In *American Control Conference*, 5055–5061. doi:10.1109/ACC.2008.4587295.

Li, Y. and Zheng, J. (2020). Real-time collision avoidance planning for unmanned surface vessels based on field theory. *ISA Transactions*, 106, 233–242. doi:https://doi.org/10.1016/j.isatra.2020.07.018.

López, J., Sanchez-Vilariño, P., Cacho, M.D., and Guillén, E.L. (2020). Obstacle avoidance in dynamic environments based on velocity space optimization. *Robotics and Autonomous Systems*, 131, 103569. doi:https://doi.org/10.1016/j.robot.2020.103569.

Masehian, E. and Katebi, Y. (2007). Robot motion planning in dynamic environments with moving obstacles

and target. *World Academy of Science, Engineering and Technology*, 29, 107–112.

Moe, S., Pettersen, K.Y., and Gravdahl, J.T. (2020). Set-based collision avoidance applications to robotic systems. *Mechatronics*, 69, 102399. doi:https://doi.org/10.1016/j.mechatronics.2020.102399.

Poonganam, S.N.J., Gopalakrishnan, B., Avula, V.S.S.B.K., Singh, A.K., Krishna, K.M., and Manocha, D. (2020). Reactive navigation under non-parametric uncertainty through Hilbert space embedding of probabilistic velocity obstacles. *IEEE Robotics and Automation Letters*, 5(2), 2690–2697. doi:10.1109/LRA.2020.2972840.

Savkin, A.V. and Wang, C. (2013). A simple biologically inspired algorithm for collision-free navigation of a unicycle-like robot in dynamic environments with moving obstacles. *Robotica*, 31(6), 993–1001. doi:10.1017/S0263574713000313.

Savkin, A.V. and Wang, C. (2014). Seeking a path through the crowd: Robot navigation in unknown dynamic environments with moving obstacles based on an integrated environment representation. *Robotics and Autonomous Systems*, 62(10), 1568–1580. doi:https://doi.org/10.1016/j.robot.2014.05.006.

Seder, M. and Petrovic, I. (2007). Dynamic window based approach to mobile robot motion control in the presence of moving obstacles. In *IEEE International Conference on Robotics and Automation*, 986–1991. doi:10.1109/ROBOT.2007.363613.

Sunkara, V. and Chakravarthy, A. (2016). Collision avoidance laws for objects with arbitrary shapes. In *IEEE 55th Conference on Decision and Control*, 5158–5164. doi:10.1109/CDC.2016.7799058.

Sunkara, V., Chakravarthy, A., and Ghose, D. (2019). Collision avoidance of arbitrarily shaped deforming objects using collision cones. *IEEE Robotics and Automation Letters*, 4(2), 2156–2163. doi:10.1109/LRA.2019.2900535.

Wiig, M.S., Pettersen, K.Y., and Savkin, A.V. (2017). A reactive collision avoidance algorithm for nonholonomic vehicles. In *IEEE Conference on Control Technology and Applications*, 1776–1783. doi:10.1109/CCTA.2017.8062714.

Xinyi, Y., Yichen, Z., Liang, L., and Linlin, O. (2019). Dynamic window with virtual goal (DW-VG): a new reactive obstacle avoidance approach based on motion prediction. *Robotica*, 37(8), 1438–1456. doi:10.1017/S0263574719000043.

Zhang, Q., Yue, S.g., Yin, Q.j., and Zha, Y.b. (2013). Dynamic obstacle-avoiding path planning for robots based on modified potential field method. In D.S. Huang, K.H. Jo, Y.Q. Zhou, and K. Han (eds.), *Intelligent Computing Theories and Technology*, 332–342. Springer Berlin Heidelberg, Berlin, Heidelberg.

Zhu, X., Yi, J., Ding, H., and He, L. (2020). Velocity obstacle based on vertical ellipse for multi-robot collision avoidance. *Journal of Intelligent & Robotic Systems*, 99, 183–208. doi:10.1007/s10846-019-01127-6.

Zhu, Y., Zhang, T., Song, J., Li, X., and Nakamura, M. (2012). A new method for mobile robots to avoid collision with moving obstacle. *Artificial Life and Robotics*, 16(4), 507–510. doi:https://doi.org/10.1007/s10015-011-0975-z.